JOURNAL OF APPLIED ELECTROCHEMISTRY 23 (1993) 1301–1309

Electrochemical regeneration of ceric sulphate in an undivided cell

J. BEEN, C.W. OLOMAN

Department of Chemical Engineering, University of British Columbia, Vancouver, BC, V6T 1Z4 Canada

Received 9 July 1992; revised 10 December 1992

Ceric sulphate (0–0.5 M) was generated electrochemically from cerous sulphate slurries (0.5–0.8 M total cerium) in 1.6 M sulphuric acid, at 50 °C, using a bench scale differential area undivided electrochemical cell with an anode to cathode ratio of eleven. A cell current efficiency for Ce(IV) of 90% was obtained at an anode current density of 0.25 A cm^{-2}. An empirical model illustrates an increase in overall current efficiency for Ce(IV) with an increase in electrolyte velocity, an increase in total cerium concentration, and a decrease in the cell current. From separate kinetic studies on rotating electrodes, both, anode and cathode kinetics were found to be affected by cerium sulphate adsorption processes. Anode adsorption of cerous sulphate species leads to inhibited mass transfer and negatively affected current efficiencies for Ce(IV). Cathode adsorption of cerium sulphate is thought to be responsible for high cathode current efficiencies for hydrogen (93–100%). The dissolved cerous sulphate concentration increased with increasing ceric sulphate and total cerium sulphate concentrations resulting in slurries with a stable dissolved cerous sulphate concentration of as high as 0.85 M in 1.6 M H_2SO_4 at room temperature.

1. Introduction

In the 1970s, the advantages of anthraquinone (AQ), or tetrahydroanthraquinone (THAQ), as an additive in the manufacture of wood pulp became apparent [1]. The use of AQ or THAQ leads to 2–3% higher pulping yields than equivalent Kraft pulping processes and results in energy savings through a reduction of the process temperature, increased pulp production and a decrease in the amount of sulphides required. Since THAQ works as a catalyst only small quantities are required. In 1980, the Canadian government approved the use of THAQ and AQ in the pulp and paper industry. Consequently, the demand is expected to grow with increasing numbers of pulp mills using the additives. At the present, the total potential market is estimated at 100 000 tonnes per year mostly consisting of the pulp and paper industry and dyestuffs [2]. One major drawback, however, is that AQ is an expensive chemical when prepared chemically employing anthracene or phthalic anhydride as its raw material and many mills are reluctant to use it for reasons of its cost-effectiveness.

Oxidation of naphthalene by Ce(IV) to produce NQ, naphthaquinone, and, subsequently, THAQ has been described and investigated by others and the process developed by W.R. Grace & Company [3, 4] has now reached the pilot plant testing phase by Hydro Quebec with a production capacity of 70 tonnes of THAQ per year [2]. The Ce(IV)/Ce(III) redox couple is often selected for indirect electro-oxidation because of the excellent selectivity of Ce(IV) for partial oxidations of organic compounds. Ce(IV) is regenerated from Ce(III) by electrooxidation.

The electrochemical cell design for the regeneration of Ce(IV) and the choice of the anion in the aqueous electrolyte still require further investigation. The preparation of Ce(IV) in an aqueous nitric acid/organic solvent emulsion in an undivided cell was studied by Pletcher and Valdes [5]. They considered the use of *in situ* extraction of the Ce(IV) into an organic solvent by means of a phase transfer agent as a way of protecting the product from reduction at the cathode. Low current efficiencies of 40% were obtained at low current densities of 0.01 A cm^{-2}.

W.R. Grace & Company have found that cerium can be dissolved at high concentrations in aqueous methanesulphonic acid [3, 4]. The use of the methanesulphonate anion with Ce(IV) avoids some of the problems associated with other ions such as undesirable organic byproducts with nitrate, chloride, and perchlorate and low solubility of cerium in sulphate or acetate solutions. Because of the high possible Ce(III) concentrations, they were able to obtain a current efficiency of 94% at an apparent current density of 0.30 A cm^{-2} in a divided electrochemical cell. The starting Ce(III) concentration was 0.88 M in 4.0 M methanesulphonic acid. The electrolyte solution is, however, quite viscous at 2.45 cSt (centistokes) giving a low diffusion coefficient. Therefore, to obtain the above results, a 3-D, reticulated iridium oxide coated titanium flow-by anode had to be used. Increasing cerium concentrations dramatically reduced the electrochemical cell cost at all cerium conversions.

The work described in this paper is an extension of

0021-891X

a BC Research project based on work by Oehr [6]. Oehr used cerous sulphate slurries to overcome the low solubility of cerous sulphate in sulphuric acid. The design of an electrochemical reactor is difficult because ceric sulphate deposition on the cathode, platinum oxide formation on the anode, and gas evolution at high current densities affect the electrode processes and give circumstances of mass transfer different to those documented in the literature. The objective of this work was to obtain electrode kinetic data, to obtain operating data from an electrochemical test cell, and to develop a reactor model.

1.1. *Reaction kinetics*

In the process of electrochemical regeneration of ceric sulphate in an undivided cell, competing reactions occur at both anode and cathode. At the anode, the primary reaction is the oxidation of cerous sulphate to form ceric sulphate. This reaction is limited by mass transfer at increased potentials. The secondary reaction is the oxygen evolution reaction which is kinetically controlled.

Anode reactions

$$Ce^{3+} \longrightarrow Ce^{4+} + e^- \qquad (1.46V \text{ vs SHE})$$

$$2H_2O \longrightarrow O_2 + 4H^+ + 4e^- \qquad (1.23V \text{ vs SHE})$$

Similarly, at the cathode, the primary reaction is the evolution of hydrogen. The reduction of Ce(IV) to Ce(III) is the secondary reaction.

Cathode reactions

$$2H^+ + 2e^- \longrightarrow H_2 \qquad (0.00V \text{ vs SHE})$$

$$Ce^{4+} + e^- \longrightarrow Ce^{3+} \qquad (1.46V \text{ vs SHE})$$

The hydrogen evolution reaction is kinetically controlled whereas the Ce(IV) reduction reaction is mass transfer controlled [7]. Consequently, the cathode current efficiency for hydrogen is promoted by high current densities whereas the anode current efficiency for Ce(IV) is promoted by low current densities. The use of a differential area cell is aimed at optimizing the cell current efficiency for Ce(IV) by producing relatively high cathode current densities together with low anode current densities in an undivided cell.

The cerium redox reaction mechanism was initially assumed by Vetter [8] to be simply

$$Ce^{4+}_{aq} + e^- \rightleftharpoons Ce^{3+}_{aq} \qquad (1)$$

It has now become apparent that cerium readily forms complexes with the solvent. Solvation explains the dependence of the redox potential on the nature and concentration of the acid medium. In 1–2 M sulphuric acid it is difficult to predict the extent of Ce(III) complexing but it is believed that Ce(III) exists in solution primarily as Ce^{3+} and $CeSO_4^+$ and to some extent as $Ce(SO_4)_2^-$ [9], [10]. The $Ce(SO_4)_3^{2-}$ complex seems to be predominantly formed by Ce(IV) [11].

2. Experimental apparatus and procedures

Electrolyte slurries were prepared by reaction of excess sulphuric acid with cerium carbonate to form cerous sulphate. The electrolyte was left to equilibrate overnight at 50 °C and the acid concentration was then adjusted to 1.6 M. The Ce (IV) concentration was determined by titration with ferrous ammonium sulphate. Analysis of dissolved Ce(III) was accomplished by filtration of the sample, oxidation to Ce(IV) using sodium bismuthate and subsequent titration with ferrous ammonium sulphate [12]. Repeating the above procedure without filtration gave the total cerium concentration.

2.1. *Anode kinetic study*

The anode kinetics was studied in a 1 dm^3 (litre) glass vessel at atmospheric pressure and 50 °C using a platinised titanium rotating disc electrode as the working electrode, WE, and a saturated calomel electrode as the reference electrode, RE.

The Ce(IV) concentration was varied from 0 to 0.5 M at a total cerium concentration of 0.56 and 0.76 M in 1.6 M sulphuric acid. Some solids were observed to be present at all concentrations and typically comprised about 7 to 10% of the total volume at low Ce(IV) concentrations and 1 to 3% of the total volume at high Ce(IV) concentrations, regardless of the total cerium concentration.

The slurry solids were kept suspended by a magnetic stirrer. The *IR*-drop was measured to be negligible. In each slurry, the electrode rotational speed was varied from 1000 to 3000, 4000, 5000, and 7000 r.p.m. At each rotational speed, the WE-potential was swept at a rate of 0.12 V min^{-1} between 0.040 V vs SHE and a potential giving a current density of 0.325 A cm^{-2}. Higher current densities were avoided due to equipment limitations.

Platinum oxide formation at high anodic potentials is a well known occurrence at platinum electrodes and can seriously affect the reaction kinetics [7, 13, 14]. To obtain a constant oxide layer, a potential program was followed after Kuhn and Randle [7, 13, 14], in which the electrode was initially cleaned by polarizing it negatively to remove any existing oxides. The electrode was then held at a positive oxidation potential, slightly positive of the anodic limit of the scanning range, for a constant time period to create a reproducible oxide layer. Since the oxygen reduction reaction has a large hysteresis effect, the oxide is not reduced and no further oxide growth occurs.

2.2. *Cathode kinetic study*

The cathode kinetics were obtained in the same glass vessel, using the same slurry concentrations at the same temperature and pressure as used in the anode study. The WE consisted now of a rotating tungsten rod with an electrode area of 1.26 cm^2. The RE was again a saturated calomel electrode. The current was

swept stepwise in increments of 0.5 A between 0.5 and 4.5 A giving cathode current densities ranging from 0.4 to 3.6 A cm^{-2}. This sweeping was repeated several times at rotational speeds of 1000 r.p.m., 3000 r.p.m. and 6000 r.p.m. The readings of 5 to 8 sweeps were averaged and used for further data analysis. The *IR*-drop was measured by current interruption and recorded on a storage oscilloscope. The high cathode currents together with the use of a saturated calomel RE resulted in a relatively slow response of the order of 50 μs. The subsequent error in the *IR*-drop is estimated to be $\sim$ 10% and does not affect any qualitative comparisons between runs.

2.3. *Laboratory electrochemical flow reactor*

Figure 1 is a flowsheet of the laboratory electrochemical flow reactor used to study the oxidation of Ce(III) in a differential area, undivided tube and wire cell. Figure 2 is a diagram of the reactor and consists of a platinized titanium pipe as the anode, 45.7 cm long and 1.387 cm inside diameter. Through the centre of this pipe runs a tungsten wire which is 0.125 cm in diameter and approximately 1 m long. The active electrode portion of the wire is also 45.7 cm long as the ends outside the reactor pipe are Teflon coated. The anode to cathode area ratio is eleven to one. Power for the reactor was supplied by a 50 A d.c. power supply.

The reactor was fed from the bottom with a cerium sulphate slurry in 1.6 M H_2SO_4 which was recycled to a sealed 20 dm^3 feed tank in a batch process. Throughout the preparation and equilibration periods of the cerium sulphate slurries, the electrolyte was circulated to prevent settling of the solids and plugging of the lines. The reactor was operated galvanostatically at 50 °C and approximately atmospheric pressure. Entrained gases were separated from the liquid slurry in the feed tank, then dried over Drierite, sampled, and analyzed.

The electrolyte flow was regulated manually to give slurry velocities in the reactor of 1.1 and 2.8 m s^{-1}. At these velocities the slurry flow is highly turbulent with Reynolds numbers of $\sim$ 14 000 and $\sim$ 35 000, respectively.

During a run, current and cell potential readings as well as product gas flow rate measurements were taken every 15 to 20 min. At the end of each hour, a liquid sample and two gas samples were taken. The liquid sample was analysed for total cerium concentration (including solids), dissolved Ce(III) concentration, and Ce(IV) concentration. The gas samples were analysed for hydrogen, oxygen, and nitrogen using a gas chromatograph. The gas analysis and the product gas flow rate were used to determine the anode and cathode current efficiencies for Ce(IV) and hydrogen.

The objective was to obtain a final Ce(IV) concentration of 0.5 M, but the current efficiency for Ce(IV) approached such low values in some cases that the run was terminated at lower concentrations. At the end of the run, 30% H_2O_2 was added to the slurry to reduce Ce(IV) to Ce(III). The slurry was circulated overnight to equilibrate at 50 °C. Excess H_2O_2 had decomposed into water and oxygen gas by the next day. The acid concentration was adjusted to 1.6 M through the addition of concentrated sulphuric acid to account for the slight increase in volume.

A total of eight runs was performed. Six runs were conducted at a high slurry velocity (2.8 m s^{-1}) with high (0.75–0.8 M) and low (0.5–0.6 M) total cerium concentrations and three levels of current density (18, 34, and 50 A total current). Two runs were performed at a low slurry velocity (1.1 m s^{-1}).

3. Results and discussion

3.1. *Dissolved cerium (III) concentration*

The solubilization of cerous ions by ceric ions in sulphuric acid media was observed by Komatsu *et al.* [15], who patented a process for electrolyzing satu-

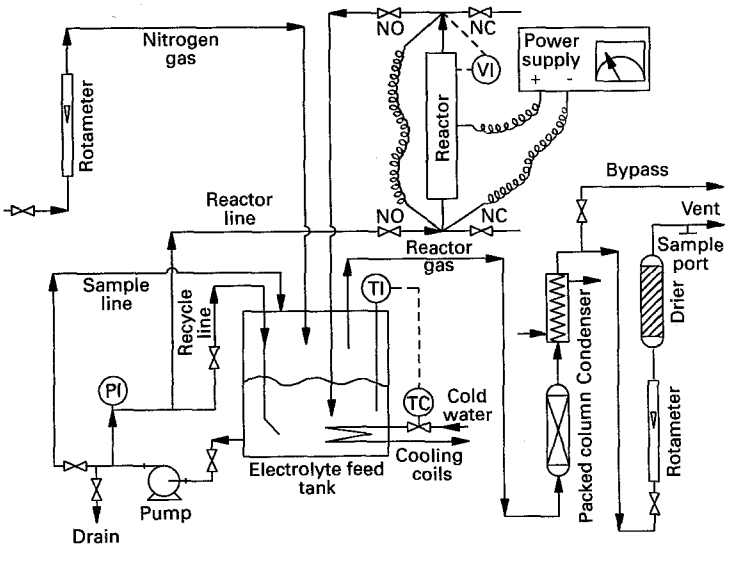

Fig. 1. Apparatus of the laboratory electrochemical reactor.

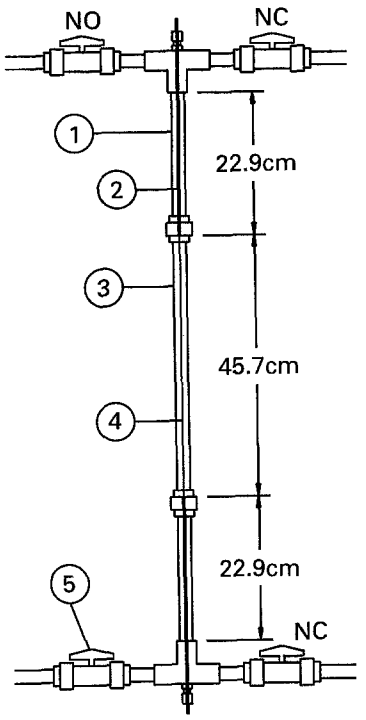

Fig. 2. Construction of the reactor. (1) 1.91 cm o/d gauge glass, (2) Teflon coated tungsten wire, (3) 1.27 cm SCH 80 platinized titanium pipe, (4) 0.125 cm o/d tungsten wire, (5) valve used to regulate flow.

rated cerous sulphate solutions in the presence of ceric sulphate. The present work appears to extend Komatsu's work in the extent to which the ceric ion solubilizes the cerous ion. During the course of the kinetic experiments it became apparent that the solubility of cerous sulphate in sulphuric acid is not only a function of the ceric ion concentration but also depends on the concentration of undissolved cerous sulphate solids. At high Ce(IV) concentrations the solubility of the cerous sulphate seemed to be limited only by the total cerium concentration. For instance, at a total cerium concentration of 0.75 M and a Ce(IV) concentration of 0.5 M, the dissolved Ce(III) concentration would typically be ~ 0.22 M with the cerous sulphate solids contributing less than 0.03 M. When the dissolved cerous sulphate concentration was not limited by the total cerium concentration, the data were analysed using a least squares curve fitting method and the dissolved Ce(III) concentration was best described by the linear equation:

$$\mathrm{Ce(III)_{dissolved}} = 0.08 + 0.36\,\mathrm{Ce(IV)} + 0.28\,\mathrm{Ce_{total}} \quad (2)$$

or

$$\mathrm{Ce(III)_{dissolved}} = 0.11 + 0.89\,\mathrm{Ce(IV)} + 0.39\,\mathrm{Ce(III)_{undissolved}}$$

with a standard deviation of 0.03 M. This equation was obtained for 0 to 0.38 M Ce(IV), 0.5 to 0.8 M total cerium and $\sim$ 0 to 0.4 M undissolved cerium at 50 °C. The cerous sulphate solubility in ceric sulphate solutions prepared from ammonium ceric nitrate in 1.6 M sulphuric acid was also predicted very well by Equation 2.

If Equation 2 were extrapolated to higher Ce(IV) and/or undissolved Ce(III) concentrations, very high concentrations of dissolved cerous sulphate might be possible. The presence of undissolved cerous sulphate solids does not necessarily indicate that the solution is saturated with cerous sulphate. At room temperature, a thermodynamically stable cerium sulphate solution, containing 1.37 M total cerium and 0.52 M ceric sulphate, was found to contain an unmeasurably small amount of cerous sulphate solids and 0.85 M dissolved cerous sulphate, which is higher than expected from Equation 2. The prospect of even higher cerous sulphate concentrations was not investigated.

The solubilization of cerous sulphate by ceric sulphate may be the result of a change in ionic strength and activity coefficients. An increase in the more strongly sulphated Ce(IV) concentration, predominantly $Ce(SO_4)_3^{2-}$, may push the dissolution equilibrium reaction to the right, increasing the dissolved cerous sulphate concentration, $Ce^{3+}CeSO_4^+$, as well as the SO_4^{2-} concentration.

More difficult to explain is the effect of solids and the presence of solids at all times even when the total cerium concentration appears to limit the cerous sulphate dissolution. At least five different cerous sulphate hydrates have been found to occur at temperatures between 0 and 100 °C ranging from dodecahydrate to tetrahydrate [16]. BC Research observed a temporary supersaturation of electrolyte with cerous sulphate upon mixing two solutions obtained from different cerous sulphate hydrates [17]. This suggests that the nature of the solid is definitely important, whereas the present study suggests that it may have a more permanent effect than was first thought. Also, a mixture of hydrates may be present, some of which may be more soluble than others, explaining the presence of a small amount of solids at all times.

3.2. *Anode kinetic study*

The oxygen evolution reaction on platinum only occurs at potentials above 1.75 V vs SHE. At lower potentials, the potentiometric curve (Figs 3 and 4) represents the cerium oxidation reaction and these points were least squares fitted to the mass transfer limited Tafel equation:

$$V = a + b\log(i_{ce}) - b\log\frac{(i_{lim} - i_{ce})}{i_{lim}} \quad (3)$$

where i_{ce} is the current density (A cm^{-2}), i_{lim} is the limiting current density (A cm^{-2}), b is the Tafel slope (V decade^{-1}), a is the Tafel intercept and includes the reversible potential (V vs SHE), and V is the potential (V vs SHE). The fitting parameters were a, b, and i_{lim}.

The Tafel slope and intercept of the cerium oxidation reaction did not vary with Ce(IV) and Ce(III) concentrations. The average values with standard deviations are:

Tafel slope (0.36 ± 0.04) V decade^{-1}

Tafel intercept (1.7 ± 0.2) V vs SHE

The limiting current density increased with an increase in rotational speed from 1000 to 3000 to 7000 r.p.m. and an increase in the Ce(III) concentration from 0.08 to 0.16 to 0.27 M (see Figs 3 and 4). The theoretical analysis of rotating disc electrode kinetics predicts a linear increase of the limiting current density with the Ce(III) concentration and with the square root of the rotational speed. The data was fitted best by the model:

$$i_{\text{lim}} = 0.046\omega^{0.31} C_b^{0.69} \quad (4)$$

where ω is the rotational speed in rad s^{-1} and C_b is the dissolved cerous sulphate concentration in M. The lower power of the rotational speed indicates inhibited mass transfer. In their studies on the cerium kinetics, Randle and Kuhn [7] also observed a reaction order in Ce(III) of less than one at Ce(III) concentrations greater than 20 mM. They attributed this to the adsorption of inactive Ce(III) species, possibly $Ce(SO_4)_2^-$ and/or $Ce(SO_4)_3^{3-}$, on the electrode which decreased the effective electrode area.

Repeated formation and reduction of oxides on the anode causes extensive electrode roughening. Using the method of Biegler [18], the surface roughness of the platinum rotating disc electrode was found to have increased by a factor of three over the duration of the research project. Yet, there was no corresponding change in current-potential values. This is also attributed to significant adsorption of cerous sulphate complexes on the electrode and supports observations made by Kuhn and Randle [7, 13] in much more dilute solutions. They observed, as we have, that the oxidation reaction is zero order in Ce(IV).

3.3. *Cathode kinetic study*

A yellow non-conductive crystal-like cerium sulphate deposit formed on the tungsten cathode in slurries with high concentrations of ceric and cerous sulphate

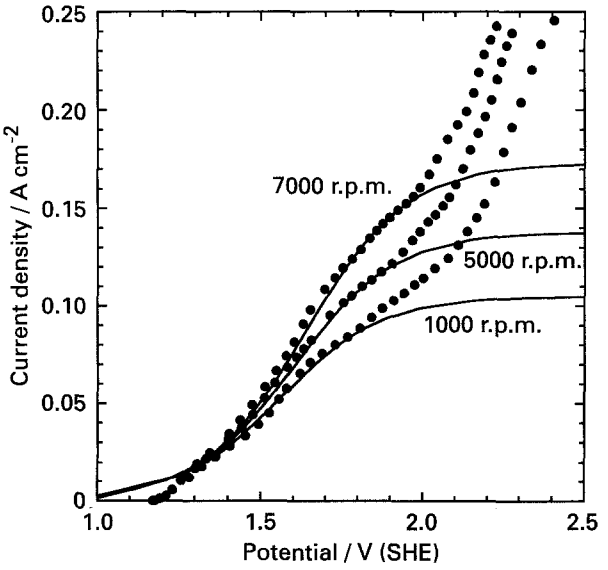

Fig. 3. Anode kinetic data: the effect of rotational speed on the limiting current density in a slurry containing 0.12 M Ce(IV), 0.28 M Ce(III), and 0.56 M total cerium. Key: (●) experimental values; (—) fitted cerium current.

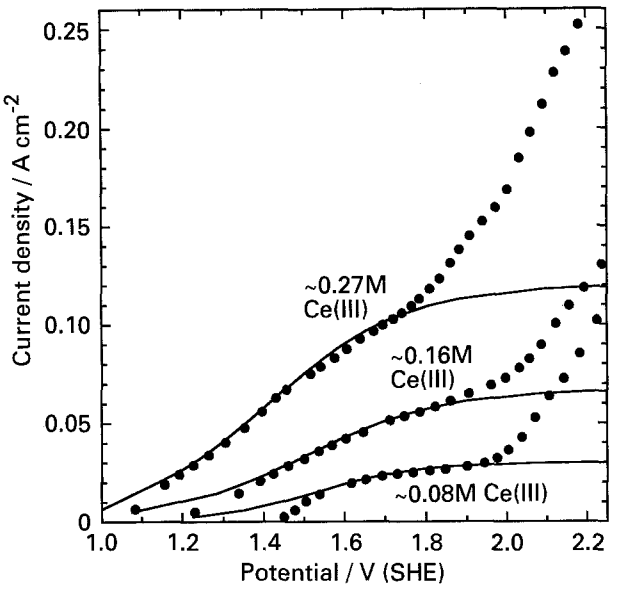

Fig. 4. Anode kinetic data: the effect of cerous sulphate concentration at 3000 r.p.m. and 0.56 M total cerium sulphate. Key: (●) experimental values; (—) fitted cerium current.

(i.e > 0.15 M). The rate of crystal formation is promoted by cathode surface roughness and hindered by highly turbulent solutions and high current densities. The electrode was repeatedly removed and cleaned when measurements were hindered by a severe deposit problem.

As illustrated in Figs 5, 6, and 7, the hydrogen evolution reaction does not follow Tafel behaviour. Harrison found that the inhibiting effect of a hydrogen bubble layer results in a change of the Tafel slope, or the charge transfer coefficient [19]. At high cerium concentrations, the adsorption of cerium sulphate species is expected to play an even greater role than the hydrogen bubbles, affecting potential values and cathode current efficiencies.

Between the potentials of zero and −0.6 V vs SHE, the current originates entirely from the mass transfer controlled cerium reduction reaction. An estimate of the current efficiency for hydrogen can be obtained if the effect of mass transfer enhancement due to increased hydrogen gas evolution at the more cathodic potentials is ignored. The limiting current density for the reduction of Ce(IV) was measured within this potential region in all slurries at rotational speeds from 1000 r.p.m. to 6000 r.p.m. The presence of a mass transfer inhibiting coating was suggested by the insensitivity of the limiting current density to rotational speed. Most of the data were obtained immediately after cleaning the electrode but in many cases the limiting current density was much lower after a period of 5–10 min. The values ranged between 0.008 and 0.066 A cm^{-2} independent of the Ce(IV) concentration. If it is assumed that the maximum limiting current density of 0.066 A cm^{-2} is the partial current density for the reduction of Ce(IV) at more cathodic potentials, then the electrode current efficiency for hydrogen is still greater than 93% in the worst case of a low current density of 1 A cm^{-2} and a high Ce(IV) concentration.

From the potentiometric data, it is observed that the potential becomes increasingly dependent on the Ce(IV) concentration (Fig 7). Interestingly, the potential is also dependent on the Ce(III) concentration, especially, when this concentration is high (Figs 5 and 6). Serious crystallization problems were only present at high Ce(III) and Ce(IV) concentrations and not in solutions with only a high concentration of Ce(IV).

It is hypothesized that at low Ce(III) concentrations, large sulphated cerium complexes with low charge densities accumulate near the cathode resulting in high potentials and mass transfer impedance without physical adsorption and deposit problems. At higher Ce(III) concentrations, the concentration of the smaller Ce^{3+} ion increases and this species, with a high positive charge density, can adsorb onto the cathode. At high Ce(III) and Ce(IV) concentrations, adsorbed Ce^{3+} ions react with $Ce(SO_4)_3^{2-}$ in an electron transfer step forming cerous sulphate deposits:

$$Ce^{3+} + Ce(SO_4)_3^{2-} + e^- \rightarrow Ce_2(SO_4)_3 \qquad (5)$$

To test the hypothesis of cerous sulphate electrode deposits, a heavy cerium sulphate deposit, formed through electrolysis, was rinsed lightly with distilled water and dissolved in sulphuric acid. As expected, the resulting solution was found to contain only Ce^{III} and no Ce^{IV}.

Deposit formation is promoted by surface roughness, as indicated by the stratified appearance of the deposit along the grooves of a rough tungsten wire and the noticeable decrease of deposit formation on a smoothly etched tungsten surface. Gas nucleation occurs more frequently on rough surfaces, enhancing local fluid circulation and facilitating the transport of Ce(IV) to the surface where it reacts with Ce(III) and is deposited. Increased local mass transfer also explains the increased rate of deposit formation at higher current densities. The local pH at the electrode only increases slightly and is not expected to be the reason for cerium sulphate deposits. Calculations based on the diffusion coefficient of the hydrogen ion, the worst-possible-case assumption of no mass transfer enhancement from generated gases, and the equation of Eisenberg, Tobias, and Wilke [20], which describes the diffusion layer thickness at rotating wire electrodes, indicated that the pH at the electrode is not expected to increase above −0.01 at the conditions of this study.

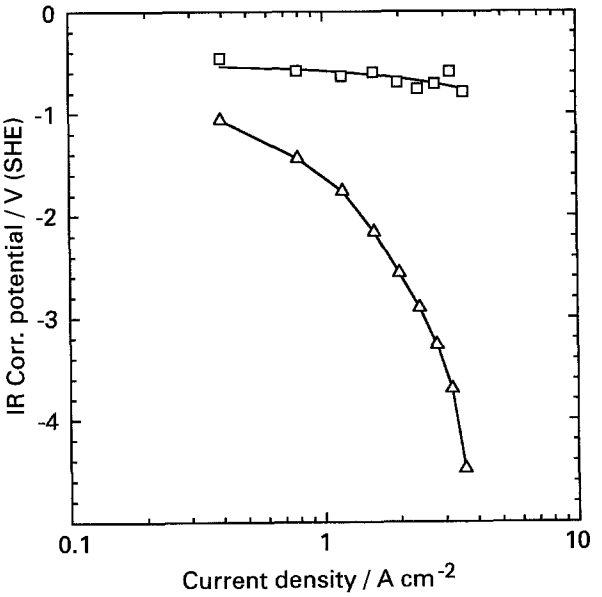

Fig. 6. Cathode kinetic data: The effect of an increasing Ce(III) concentration in the presence of 0.5 M Ce(IV). Key: (□) 0.56 M; (△) 0.76 M total cerium.

3.4. *Laboratory electrochemical flow reactor*

Figures 8 to 11 illustrate the test results of the electro-

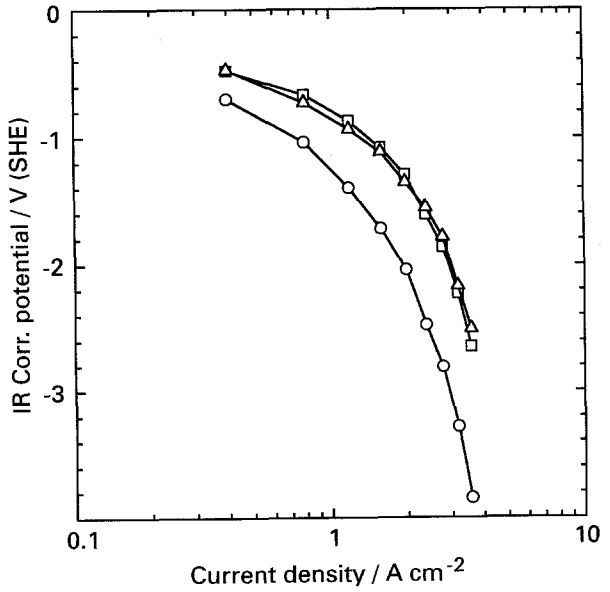

Fig. 5. Cathode kinetic data: The effect of an increasing Ce(III) concentration in the absence of Ce(IV) Key: (□) 0.19 M; (△) 0.50 M; (○) 0.76 M total cerium.

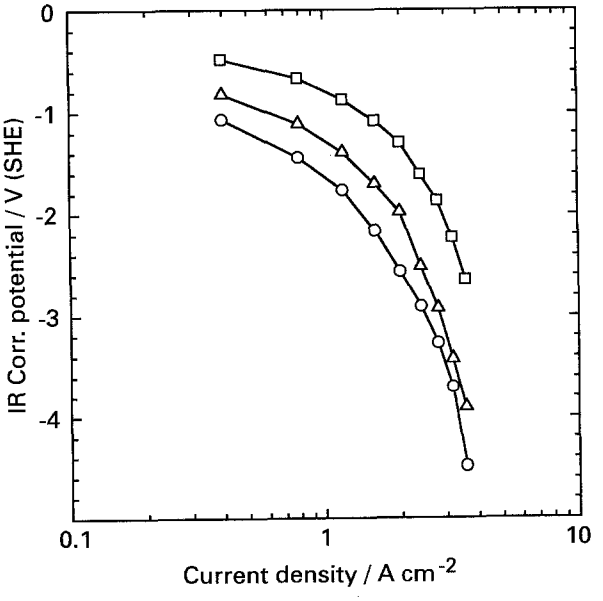

Fig. 7. Cathode kinetic data: The effect of an increasing Ce(IV) concentration at a constant dissolved Ce(III) concentration of ~ 0.2 M. Key: (□) 0 M Ce(IV), 0.19 M total cerium; (△) 0.29 M Ce (IV), 0.56 M total cerium; (○) 0.51 M Ce(IV), 0.76 M total cerium.

chemical flow reactor. The current efficiencies for Ce(IV) obtained from the gas analysis are in good agreement with the data from the concentration analysis. For illustration purposes, a least squares fitted current efficiency line has been drawn through the data.

The cathode current efficiency for hydrogen, as determined from the product gas flow rate and chromatographic analysis, was equal to 100% with an experimental error of 10% in all runs, independent of the Ce(IV) concentration.

The effect of an increased electrolyte velocity is illustrated in Fig. 8 at a high total cerium concentration and 34 A total current and in Fig. 9 at a lower total cerium concentration and 50 A total current. In Fig. 8, throughout the entire Ce(IV) concentration range, the overall current efficiency for Ce(IV) is $\sim 30\%$ higher at a velocity of $2.8\,m\,s^{-1}$ than at $1.1\,m\,s^{-1}$. The observed plateaus are due to a constant concentration of dissolved cerous sulphate despite an increasing ceric sulphate concentration. After 0.35 M Ce(IV), the dissolved Ce(III) concentration decreases and the current efficiency falls due to mass transfer dependence. This feature is also apparent at higher current densities (Fig. 9). In Fig. 9, the fall in current efficiency is more dramatic at 0.51 M than at 0.60 M total cerium due to a more rapidly decreasing Ce(III) concentration. At low Ce(IV) concentrations, the higher velocity leads again to $\sim 30\%$ higher current efficiencies for Ce(IV).

Figure 10 shows the effect of an increased total cerium concentration at $2.8\,m\,s^{-1}$ and an anode current density of $0.25\,A\,cm^{-2}$. At low Ce(IV) concentrations the measured current efficiencies for Ce(IV) are the same at $\sim 90\%$. At the lower total cerium concentration, the dissolved Ce(III) concentration

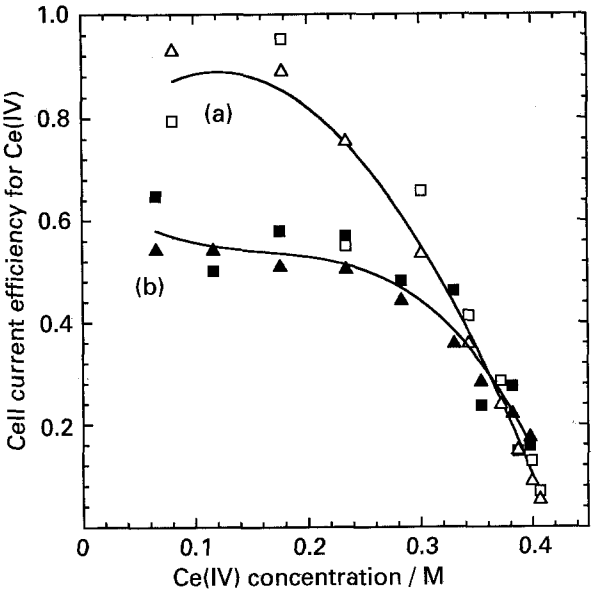

Fig. 9. Reactor data: the effect of an increased electrolyte velocity at 50 A total current or an anode current density of $0.25\,A\,cm^{-2}$. (a) $2.8\,m\,s^{-1}$, 0.51 M total cerium, (b) $1.1\,m\,s^{-1}$, 0.60 M total cerium. Key: as for Fig. 8.

falls more rapidly as does the current efficiency for Ce(IV).

In Fig. 11, the effect of current density on current efficiency for Ce(IV) is nicely illustrated at 0.51 M total cerium and an electrolyte velocity of $2.8\,m\,s^{-1}$. At a total current of 50 A (anode current density of $0.25\,A\,cm^{-2}$), the current efficiency for Ce(IV) is consistently lower than at 18 A (anode current density of $0.09\,A\,cm^{-2}$).

There was no indication of a crystalline deposit on the cathode, which is attributed to an erosive effect of the electrolyte velocity. The reactor Reynolds' numbers are much higher than those in the kinetic

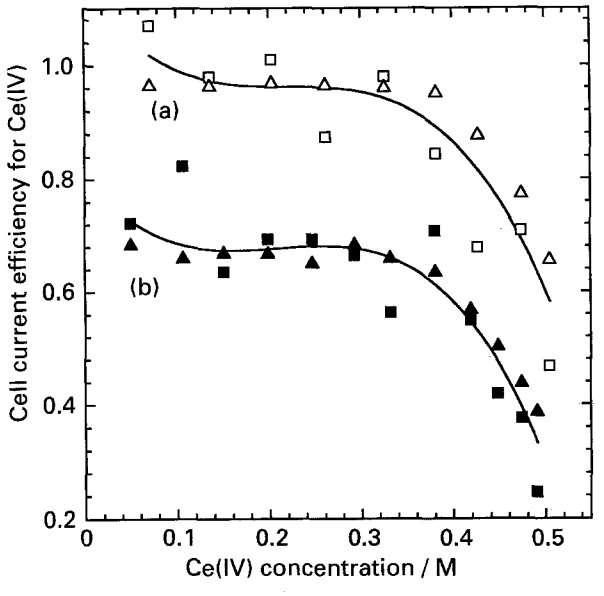

Fig. 8. Reactor data: the effect of an increased electrolyte velocity at 34 A total current or an anode current density of $0.17\,A\,cm^{-2}$. (a) $2.8\,m\,s^{-1}$, 0.82 M total cerium, (b) $1.1\,m\,s^{-1}$, 0.75 M total cerium. Key: (■) and (□) concentration analysis; (▲) and (△) gas analysis; (—) fitted current efficiency.

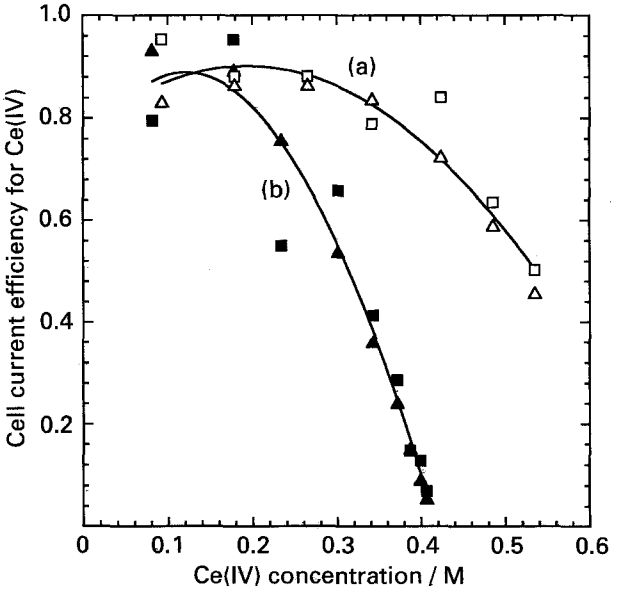

Fig. 10. Reactor data: the effect of an increased total cerium concentration at an anode current density of $0.25\,A\,cm^{-2}$ and an electrolyte velocity of $2.8\,m\,s^{-1}$. (a) 0.75 M total cerium, (b) 0.51 M total cerium. Key: as for Fig. 8.

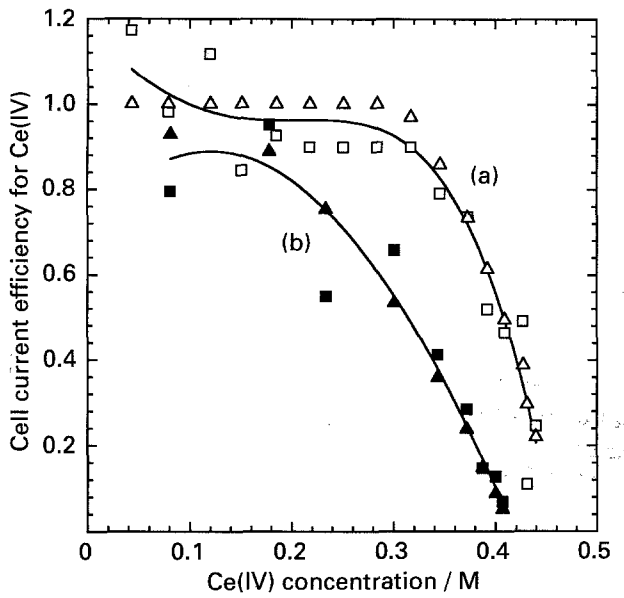

Fig. 11. Reactor data: the effect of an increased current density at 0.51 M total cerium and an electrolyte velocity of 2.8 m s^{-1}. A total current of 18 and 50 A corresponds to an anode current density of 0.09 and 0.25 A cm^{-2}, respectively. (a) 18 A, (b) 50 A. Key: as for Fig. 8.

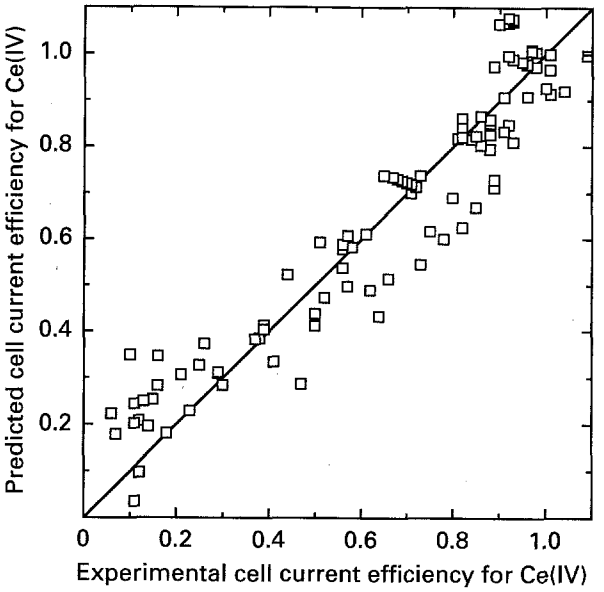

Fig. 12. The current efficiencies for Ce(IV) as predicted by Equation 6 against the values obtained experimentally.

runs. A velocity of 2.8 m s^{-1} corresponds to approximately 17 500 r.p.m. using the equation of Eisenberg, Tobias, and Wilke [20]. There was no evidence of anode or cathode wear over the ~ 400 h operating period.

The obtained data were modelled empirically:

$$CE = 0.49 + 0.14\,Veloc + 1.8\,Ce^{III} - 1.1\,Ce^{IV} - 0.3\,Ce_{solids} - 1.6\,i_{total} \quad (6)$$

CE is the overall differential current efficiency for the production of Ce(IV).

Veloc is the velocity of the slurry through the reactor (m s^{-1}).

Ce^{III} and Ce^{IV} are the dissolved cerous and ceric sulphate concentration (M).

Ce_{solids} is the amount of cerium sulphate solids obtained by subtracting Ce^{III} and Ce^{IV} from the total cerium concentration (M).

i_{total} is the total anode current density (A cm^{-2}).

The standard deviation is 0.1 in the current efficiency. Figure 12 illustrates the fit of the correlation. Equation 6 is valid for the conditions of the experimental runs i.e. for 0 to 0.54 M Ce(IV), 0.05 to 0.43 M Ce(III), 0.5 to 0.82 M total cerium in 1.6 M sulphuric acid at 50 °C and atmospheric pressure. The valid cathode current density range lies between 1 and 2.8 A cm^{-2} with a corresponding anode current density between 0.09 and 0.25 A cm^{-2} at an anode to cathode ratio of 11. The slurry velocity ranges between 1.1 and 2.8 m s^{-1}.

The slurry velocity and the cerous sulphate concentration have a positive effect on the current efficiency for Ce(IV). The ceric sulphate concentration and the current density have, as expected, a negative effect. It is interesting to note that the positive effect of cerous sulphate is stronger than the negative effect of ceric sulphate. The negative effect of solids suggests that adhesion of the solids to the anode impedes the mass transfer controlled regeneration of Ce(IV).

4. Conclusions

Ceric sulphate was successfully regenerated electrochemically from cerous sulphate slurries in 1.6 M sulphuric acid using a bench scale undivided, differential area electrochemical reactor in a batch recirculating process. Cell current efficiencies for Ce(IV) up to 90% were obtained at an anode current density of 0.25 A cm^{-2}.

Kinetic experiments at a rotating platinised titanium disc as the anode or a rotating tungsten rod as the cathode were conducted to obtain the electrode kinetics. The anode kinetic study indicated an inhibition of mass transfer at the anode by the presence of undissolved cerous sulphate solids in the slurry. This may be attributed to an affinity of these solids to adhere to the electrode. The reaction order in Ce(III) was found to be less than one, which is probably due to adsorption of anionic or polar cerous sulphate species.

In the cathode kinetic studies, a mass transfer inhibiting coating appears to be present even at low current densities leading to a very small partial current density of the cerium reduction reaction. The electrode current efficiency for hydrogen was never observed to be lower than 94%. Further deposition of crystalline cerous sulphate, promoted by surface roughness, low velocities and high concentrations of cerous and ceric sulphate, resulted in increased cathode potentials.

The observations of high cathode current efficiencies for hydrogen and a negative effect of solids on

the current efficiency for Ce(IV) were supported by the flow reactor runs. An entirely empirical approach to the results of the flow reactor runs illustrated the effects of electrolyte velocity, Ce(IV) concentration, total cerium concentration (including undissolved Ce(III)), and superficial current density on the cell current efficiency for Ce(IV).

The dissolved cerous sulphate concentration was found to be a function of the dissolved ceric sulphate concentration as well as the undissolved cerous sulphate concentration. A linear relationship was developed for the conditions of the experimental runs. In addition, a thermodynamically stable slurry was prepared at room temperature containing as much as 0.85 M dissolved cerous sulphate in 1.6 M sulphuric acid. At high ceric sulphate concentrations, the solubility of cerous sulphate appears to be limited by the total cerium concentration and the presence of a small quantity of solids is not indicative of a saturated cerous sulphate solution. Filtration might be employed to remove the solids, which are thought to be insoluble cerous sulphate hydrates, and the resulting concentrated cerous sulphate solution could be used and recycled for the regeneration of ceric sulphate.

These high cerous sulphate concentrations in sulphuric acid together with high cathode current efficiencies for hydrogen, even in the presence of high ceric sulphate concentrations, make the electrochemical regeneration of ceric sulphate in an undivided cell feasible. A high current efficiency for Ce(IV) at high anode current densities reduces the electrochemical cost and, consequently, the production cost of THAQ. Capital and energy costs are kept low in an undivided cell, and cerium sulphate deposit formation on the electrodes was not a problem at the conditions of these experiments.

Further research is required to explore the possibilities of using concentrated cerous sulphate solutions in sulphuric acid with high concentrations of ceric sulphate and to investigate the long term effects of these high concentrations on the formation of cerium sulphate deposits on the electrodes.

References

[1] T. I. Tenn, *Chem. Eng. NY* **86** (Dec 3, 1979) 64–65.
[2] S. Harrison, R. Labrecque and A. Theoret, 'Hydro-Quebec's Development and Demonstration Activities in Electro-organic synthesis', Proceedings of the Fifth International Forum On Electrolysis, Ft. Lauderdale, FA, Nov. 1991, Electrosynthesis Company, East Amherst, NY (1991).
[3] R. M. Spotnitz, R. P. Kreh, J. T. Lundquist, and P. J. Press, *J. Appl. Electrochem.* **20** (1990) 209–215.
[4] P. Pichaichanarong, R. M. Spotnitz, R. P.Kreh, S. M. Goldfarb, and J. T. Lundquist, 'Simulation of a mediated electrochemical process,' 1988 Spring National Meeting of the AIChE, New Orleans, Mar 1988, AIChE, New York, NY, preprints (1988).
[5] D. Pletcher and E. M. Valdes, *Electrochim. Acta* **33** (4), (1988) 509–515.
[6] K. H. Oehr, *Can. Patent 1 166 600* (1984).
[7] T. H. Randle and A. T. Kuhn, *J. Chem. Soc., Faraday Trans. I* **79** (1983) 1741–1756.
[6] K. J. Vetter, 'Electrochemical Kinetics', Academic Press, New York (1967).
[9] L. A. Blatz, *J. Phys. Chem.* **66** (1962) 160–164.
[10] T. W. Newton and G. M. Archand, *J. Am. Chem. Soc.* **75** (1953) 2449–2453.
[11] T. J. Hardwick and E. Robertson, *Can. J. Chem.* **29** (1951) 828-837.
[12] A. I. Vogel, 'Textbook of Quantitative Inorganic Analysis', Longman, New York (1978).
[13] T. H. Randle and A. T. Kuhn, *Electrochim. Acta* **31**(7), (1986) 739–744.
[14] A. T. Kuhn and T. H. Randle, *J. Chem. Soc. Faraday Trans. I* **81** (1985) 403–419.
[15] T. Komatsu, S. Numata, K. Hioki, T. Sumino, *US Patent* 4 530 745 (1984).
[16] J. W. Mellor, 'A Comprehensive Treatise on Inorganic and Theoretical Chemistry', Volume V, Longmans, Green & Co., New York (1924).
[17] Personal communication with K. H. Oehr.
[18] T. Biegler, D. A. J. Tand, and R. Woods, *J. Electroanal. Chem. Interfacial Electrochem.* **29** (1971) 269–277.
[19] J. A. Harrison and A. T. Kuhn, *ibid.* **184** (1985) 347–356.
[20] M. Eisenberg, D. W. Tobias, and C. R. Wilke, *J. Electrochem. Soc.* **101**(6), (1954) 306–319.